Hybrid unipolar-bipolar system with quasi-polarized code for free-space optical communication

Eddy Wijanto, Kevin Sutanto
Department of Electrical Engineering, Faculty of Engineering and Computer Sciences, Universitas Kristen Krida Wacana, Jakarta, Indonesia

Article Info	ABSTRACT
	In this study, the hybrid unipolar-bipolar (U-B) optical code division multiple access (OCDMA) with mixed unipolar-bipolar scheme in free-space optical communication was proposed. Additionally, the codeword assigned introduced the quasi-polarized code, which could be used to transmit both the unipolar and bipolar section. Using OptiSystem simulations, the model was studied. According to the results from the simulation, the proposed hybrid U-B OCDMA can correctly decode the original optical signal from its matching encoder. Further testing of the hybrid U-B OCDMA system was conducted in turbulence conditions. According to the simulation results, walsh-zero cross correlation (ZCC) performs better than all other codes for the unipolar segment whereas walsh-hadamard (W-H) code performs best for the bipolar section. The simulations also showed that the performance deterioration of the walsh-ZCC algorithm was the greatest. *This is an open access article under the [CC BY-SA](#) license.*

Corresponding Author:

Eddy Wijanto
Department of Electrical Engineering, Faculty of Engineering and Computer Sciences
Universitas Kristen Krida Wacana
Jakarta, Indonesia
Email: eddy.wiyanto@ukrida.ac.id

1. INTRODUCTION

Sixth-generation (6G) mobile network technology has high requirements to make the network more intelligent, super low latency, super-fast communication speeds, and support for a wide range of applications [1]. The smart cities, industry 4.0, e-health, wearable technology, smart utilities, and many more applications require denser networks with greater availability and coverage, including the internet of things (IoT) [2]. The most frequently researched technologies at the moment are primarily air-space-earth-sea integration, terahertz (THz), millimeter-wave (mmWave), and visible light resources, as well as wireless access solutions [3]. Due to their inherent qualities, which include the ability to offer high-capacity and low-latency connections, optical fiber technology is the best alternative to meet the requirements [4].

However, laying optical fiber connections for clients in a variety of applications is incredibly expensive, especially in the last mile. In this case, wireless communication becomes one of the prospective solutions. Congested frequency spectrum has become a significant obstacle in the development of wireless communication, particularly in the availability to middle to short-distance mobile communication [5]. In contrast, conventional radio frequency (RF) suffers from electromagnetic interference (EMI) constantly and has poor secrecy. This is especially true in settings with a lot of electronic devices, such as data centers, airports, and hospitals. As the need for high-speed and high-density data transmission grows along with the advancement of semiconductor illumination, a new wireless communication technique called optical wireless communication (OWC), which has higher dependability, a larger capacity, and a faster data-rate, is gradually

being proposed and is anticipated to break the bottleneck [6]. In contrast to traditional RF communications, OWC covers the wavelength band from ultraviolet to near-infrared (NIR) light [7]. OWC is the best short-range high-speed wireless access and effectively complements RF [8]. Further development of free-space optical (FSO) communication found the major obstacle of power attenuation caused by atmospheric turbulence in a variety of weather circumstances, yet with comparable data-rates and severely low error-rates when compared to optical fiber connections, it has become one of the most used approaches. Multiplexing technology plays a significant role in FSO communication to support dense networks. The most regular multiplexing technique in the optical system is wavelength division multiplexing (WDM), which enables the use of various light wavelengths to transmit data over a single channel. The WDM's detrimental restriction is its bandwidth efficiency. The enhancement of WDM performance is the subject of numerous studies. The dispersion correction technique for the dense WDM (DWDM) system was proposed by Gopalan *et al.* [9]. In general, nonlinearities like cross-phase modulation, self-phase modulation, and four-wave mixing affect the system. Another study recommended WDM-radio over free space optics (RoFSO) augmentation using dual FSO channel in order to reach a high capacity of 160 Gbps [10].

Meanwhile, time division multiplexing (TDM) is another multiplexing technology that can be used to improve the spectral efficiency of optical networks. This technique, which separates a single band into time slots, is effective for high-speed communications and compressed video [11]. The hybrid system, which combines optical code division multiple access (OCDMA) with time-division multiplexed passive optical network (TDM-PON) technology, was proposed in [12] order to improve the number of concurrent users. Also examined in [13] were the nonlinear optical loop mirror (NOLM), which serves as a demultiplexer, and the effects of fiber dispersion on the performance assessment of high-speed OTDM systems. The results illustrated that fiber scattering, the inalienable NOLM's crosstalk, and the exchanging profile of the control beat had an effect on the bit error-rate (BER) of the framework [13].

Another interesting multiplexing strategy to offer high-speed connectivity with large bandwidth is OCDMA, which is rising in favor in the optical communication because its asynchronous scalability, transmission, security, and flexibility. Further, with fixed in phase cross-correlation, spectral amplitude coding (SAC), one of the OCDMA methods, is proposed to reduce the effects of multi-user interference and phase induced intensity noise (PIIN) [14]. Since OCDMA systems demand the maximum auto-correlation and minimum cross-correlation detection technique, OCDMA loses its immunity to noise as a result of non-ideal correlation. Bouhezila *et al.* [15] using a novel decoder architecture appropriate for SAC-OCDMA systems with fixed correlation zone (FCZ) codes. Further, a revolutionary FSO system was proposed in [16] by fusing OFDM with SAC-OCDMA. The SAC-OCDMA system employs single photodiode detection (SPD) as the detection method and enhanced double-weight (EDW) codes as the signature codes [16]. The suggested paradigm has the potential to be developed into a flexible and effective system [16]. In terms of optical signal demodulation schemes, OCDMA can be classified into coherent and non-coherent. Non-coherent OCDMA system uses light intensity to encode optical information. Unipolar encoding, which is often used, offers the benefits of being easy to use and affordable but only works for low data-rates, like speech data. Coherent systems, on the other hand, use a matching filter to alter an optical signal's phase in order to encrypt the phase of the input light. The coherent OCDMA's superior correlation to the non-coherent approach is demonstrated by the auto-correlation intensity in the coherent system following square-law detection with the photodetector. The advantages of bipolar coding in terms of spectrum efficiency are advantageous to the coherent system [17]. As a result, for high-speed data transfer and real-time applications, bipolar coding can be applied. For coherent and incoherent sources, a performance comparison of the three unipolar codes-prime sequence (PS), quadratic codes (QC), and extended quadratic codes (EQC)-shows that the EQC codes perform better in terms of BER than the other family codes [18]. For SAC-OCDMA systems operating with incoherent sources, Al-Khafaji *et al.* [19] assess the spectral efficiency of unipolar and bipolar encoding while taking intensity noise into consideration as the main noise source. The zero cross correlation (ZCC) code can accommodate a large number of users and provides the highest possible spectral efficiency when compared to other SAC codes, according to analytically calculated equations and findings [19].

The most stable parameter that can produce twice efficiency is the polarization state of a light beam that is traveling through the atmosphere. In the polarized system, polarization domain resource still has the ability to deliver a higher multiplexing gain. Effectively suppressing PIIN is a spectral-polarization coding (SPC) OCDMA advantage. In our earlier research, the bipolar data were produced using the horizontal and vertical polarization states. The optical signals are polarized using the switch as user data and decoded using a set of fiber bragg gratings (FBGs) and optical circulators. The proposed technique effectively decreases multiple access interference (MAI) in FSO communication systems. The system's low transmission rate was a result of the system flaws induced by the optical switch's speed constraint [20]. In our later work [21], we suggested to use a bipolar optical code division multiple access (Bi-OCDMA) strategy with two electro-optical modulators (EOMs) to improve transmission rate and SPC performance. The specifications of two EOMs must also be kept as similar as feasible in order for this method to work, as the suggested system only sends the signal

with wavelength matching chip "1" in the signature code [21]. Our subsequent research developed a Bi-OCDMA method based on SAC by implementing polarization coding through an FSO channel employing a phase modulator [22]. According to the simulation results, the walsh-hadamard (W-H) code performs better than other codes. The outcomes demonstrate that the suggested Bi-OCDMA technique for a medium-distance FSO can implement the multi diagonal (MD) code [22]. The performance of wireless optical communication is also impacted by the channel impairments, which include atmospheric situations and turbulence fading, in addition to the system architecture. Islam and Majumder [23] analyze the effects of air turbulence on the BER performance of an OCDMA FSO link using an optical domain encoder and a balanced photodetector receiver outfitted with sequence inverse keying (SIK). According to the findings, the penalty is determined to be 9 dB and 11.5 dB, respectively, for BER equal to 10^9 for a link distance of 3000 m with users' number 2 and 16. For a specific code length, the maximum number of concurrent users at a given BER is also established [23]. Various signature codes for SAC-OCDMA have also been suggested and researched in numerous studies. The simulation in this research uses a number of well-known SAC codes with quasi-polarized scheme.

In this paper, a hybrid unipolar-bipolar system for FSO communication is implemented by combining the unipolar and bipolar OCDMA scheme to simultaneously send the information data. The key contributions of this research are as:

−   This paper proposed a hybrid unipolar-bipolar (U-B) OCDMA system that optimized the advantages of unipolar and bipolar scheme. This hybrid system can be used to transmit both high and low data-rates simultaneously.

−   This study presented a simple, affordable, and moderate security hybrid OCDMA system for wireless optical communication. The SAC-OCDMA principles are upheld in the proposed system, which solves the MAI issue.

−   A novel quasi-polarized SAC codes was introduced in this work to be implemented in the hybrid U-B OCDMA scheme.

−   With various SAC-OCDMA codes, the suggested system was examined in extreme weather situations under turbulence fading scenarios, and performance comparisons between various SAC-OCDMA were made. The quality factor (Q-factor) and BER performance measurements were made for additive white gaussian noise (AWGN) and AWGN with fading channel, respectively.

The following section is organized as: the suggested hybrid U-B OCDMA system with quasi-polarized code is introduced in section 2, further with the encoding and decoding structure, the prove of the correlation function, and the hybrid U-B system's quasi-polarized code. The simulation results are presented in section 3 along with information about the system's viability, performance evaluation, and a comparison of hybrid U-B OCDMA systems under extreme weather situation in the AWGN and turbulence channels, respectively. The final results of the work, as well as planned future work, are presented in section 4.

2.   RESEARCH METHOD

A common FSO channel will be used to transmit both unipolar and bipolar data signals simultaneously in the proposed hybrid U-B OCDMA system. For both unipolar and bipolar transmitters, a pseudo-random bit sequence (PRBS) is used to construct each user's data. For the unipolar encoder, Mach-Zehnder modulator was applied to modulate the information signal from PRBS according to the signature code. Direct detection technique was used in the decoding-end of unipolar receiver. The phase-modulator system suggested in [22] was implemented using the bipolar encoder. The modulation signal in the bipolar section was produced using a phase-shift keying (PSK) pulse generator, electrical bias, and electrical gain. Each user's data bit is converted into an optical signal for processing by a phase modulator, and then sent across an FSO channel to the decoder end. Devices for polarization shift keying are polarization splitters. Using a balanced photo-detection strategy, to lower the MAI, we used an optical circulator and numerous uniform FBG.

The system was tested with three users' scheme, one user sent information with unipolar scheme, while other with bipolar scheme. In this proposed hybrid U-B OCDMA system, the signature code is divided into two parts, one part used for unipolar transmission, while other for bipolar transmission. This scheme of code is namely quasi-polarized code in the rest of this paper. The feasibility of hybrid U-B OCDMA system was verified with a W-H code due to its advantageous orthogonal characteristic. The W-H matrix design was adopted from that in [24].

$$H_1 = \begin{bmatrix} 1 & 1 \\ 1 & -1 \end{bmatrix} \, and \, H_n = \begin{bmatrix} H_{n-1} & H_{n-1} \\ H_{n-1} & -H_{n-1} \end{bmatrix}, n = 2, 3, 4, \dots, \tag{1}$$

The k-th row of the matrix represents the k-th optical codeword of the W-H code given to the k-th user, and N is 2^n and denotes the length of the W-H code. The matrix of the proposed W-H code can be represented as for the bipolar section for $N=4$ [22]:

$$H_2 = \begin{bmatrix} 1 & 1 & 1 & 1 \\ 1 & -1 & 1 & -1 \\ 1 & 1 & -1 & -1 \\ 1 & -1 & -1 & 1 \end{bmatrix} = \begin{bmatrix} 1 & 1 & 1 & 1 \\ 1 & 0 & 1 & 0 \\ 1 & 1 & 0 & 0 \\ 1 & 0 & 0 & 1 \end{bmatrix} - \begin{bmatrix} 0 & 0 & 0 & 0 \\ 0 & 1 & 0 & 1 \\ 0 & 0 & 1 & 1 \\ 0 & 1 & 1 & 0 \end{bmatrix} = C_V - \overline{C}_H \tag{2}$$

the following correlation results must be reached [22] in order to employ W-H codes of length N in the bipolar schemes.

$$\theta_{hh}(k, l) = \sum_{i=1}^{N} (c_{kV}(i) - \overline{c}_{kH}(i))(c_{lV}(i) - \overline{c}_{lH}(i)) = \begin{cases} N, k = l \\ \frac{N}{2}, k \neq l \end{cases} \tag{3}$$

$$\theta_{h\overline{h}}(k, l) = \sum_{i=1}^{N} (c_{kV}(i) - \overline{c}_{kH}(i))(\overline{c}_{lV}(i) - c_{lH}(i)) = \begin{cases} 0, k = l \\ \frac{N}{2}, k \neq l \end{cases} \tag{4}$$

Table 1 shows the W-H code of length 8 with quasi-polarized scheme. Optical signals with horizontal and vertical polarization states are denoted by the letters H and V, respectively. In Figure 1, the proposed encoder's design is shown. It consists of three-continuous-wave (CW) laser arrays as the light source, two PRBS generators as the bit sequence generator, two sets of electrical bias, electrical gain, and PSK pulse generators as the modulation signal for the phase modulator, two phase modulators for optical bipolar signals modulation, a Mach-Zehnder modulator for unipolar signals modulation, four optical couplers, several optical adders.

Table 1. Walsh-hadamard codes with quasi-polarized scheme

User	Signature code	Data bit	Optical polarized signal				Optical un-polarized signal	
			H		V			
#1	1 0 1 0 1 0 1 0	0	λ_1	λ_3	λ_2	λ_4	−	
		1	λ_2	λ_4	λ_1	λ_3	λ_5	λ_7
#2	1 1 0 0 1 1 0 0	0	λ_1	λ_2	λ_3	λ_4	−	
		1	λ_3	λ_4	λ_1	λ_2	λ_5	λ_6
#3	1 0 0 1 1 0 0 1	0	λ_1	λ_4	λ_2	λ_3	−	
		1	λ_2	λ_3	λ_1	λ_4	λ_5	λ_8

For the unipolar section, one CW laser arrays emit the wavelengths according to the codeword. In the unipolar scheme, only the wavelength assigned to the "1" in the codeword will be modulated with the modulator and transmitted. Further for the bipolar section, two CW laser arrays are used in the bipolar section to emit certain wavelengths in accordance with the assigned codeword. Depending on the users' data bit of the codeword's "0" or "1," the CW laser array#1 (or #2) produces the wavelength associated with chip "1" (or "0"). As can be seen in Table I, when user#1 is given the W-H codeword X1=[1 0 1 0], the wavelengths of CW laser array#1 and #2 are (λ_1, λ_3) and (λ_2, λ_4), respectively. The PSK pulse generator is responsible for producing the electrical signals, according to the user data bit. Electrical bias and electrical gain were used to normalize the PSK pulse generator's in-phase output, which is -1 and 1, into 0 and 1 for the phase modulator's modulating signal. The electrical signal was then transferred to the EOM for modulation of optical signals. The phase modulator's output optical signals can be expressed as [22]:

$$E_{out,PM}(t) = E_{in,PM}(t). \exp(j. \Delta Q. X(t)) \tag{5}$$

where ΔQ is the phase deviation, $X(t)$ is the electrical input, and $E_{in,PM}$ represents the electrical input signal. Depending on the user data bit, the modulated signals are subsequently routed to outputs of optical coupler. The optical coupler's output can be seen as [22]:

$$\begin{pmatrix} E_{1out,C} \\ E_{2out,C} \end{pmatrix} = \begin{pmatrix} \alpha\sqrt{1-c} & pj\sqrt{c} \\ pj\sqrt{c} & \sqrt{1-c} \end{pmatrix} \begin{pmatrix} E_{1in} \\ E_{2in} \end{pmatrix} \tag{6}$$

where E_{in} is the input optical signal, p is the conjugate parameter, c is the coupling coefficient, and α represents the additional loss. For user's data bit of "1", the signals will appear only on the first output of the optical couplers, further being polarized into horizontal polarization state in the upper polarization and vice versa. These polarized signals are then combined using the polarization combiner.

The proposed hybrid U-B OCDMA decoder's structure is shown in Figure 2. The framework from the single-user situation can be enlarged to the higher multi-user scheme. It includes a polarization splitter, two optical circulators, three set of uniform FBGs for the unipolar and bipolar sections, three optical adders, three photo-detectors, three low pass Bessel filters, and one electrical subtractor to complete the unipolar and bipolar scheme. The unipolar section implements direct detection, and the bipolar section applies balanced photo-detection with the subtraction of the upper and lower signals in order to reduce the MAI.
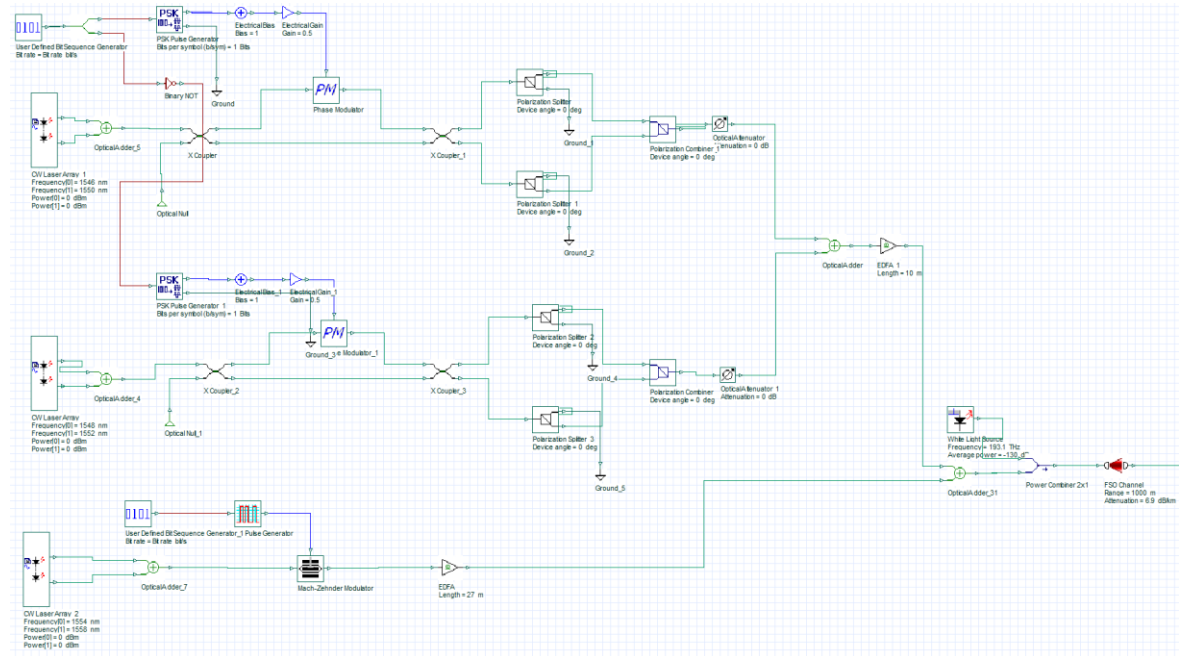
Figure 1. Proposed hybrid U-B OCDMA encoder with quasi-polarized code
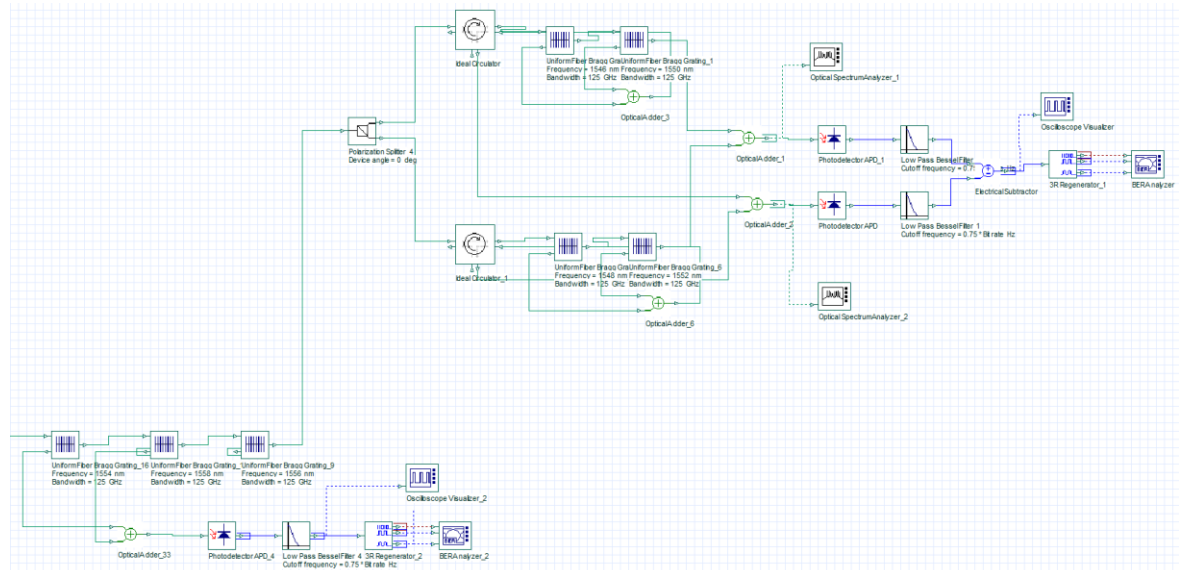
Figure 2. Proposed hybrid U-B OCDMA decoder with quasi-polarized code

The signals received by decoder firstly filtered with uniform FBG to reflect the wavelength assigned for unipolar section. The remain wavelength further passing through polarization splitter. Before transmitting the incoming optical signals to the following two circulators, whose port #2 are connected to two separate

series of uniform FBGs, respectively, the polarization splitter in the bipolar section depolarizes them. The wavelengths of these series of uniform FBGs is identified by the codewords. The upper optical adder collects the transmitted signals of the two series of uniform FBGs while port #3 of the circulator receive the reflected signals. The optical signals of the two optical circulators is gathered by the lower optical adder [22].

The data bit of the desired user is lastly determined using a 3R regenerator. The BER analyzer was then used to measure the BER and Q-factor (Q-F). Mathematically, the suggested BER can be assessed using:

$$BER = \frac{1}{2} erfc\left(\sqrt{\frac{SNR}{2}}\right) \qquad (7)$$

where *SNR* stands for the proposed system's signal-to-noise ratio and *erfc* stands for the complementary error function in time, which may be found by:

$$erfc = \frac{2}{\sqrt{\pi}} \int_x^\infty exp(-t^2)\, dt \qquad (8)$$

in order to make the examination of the system performance in this simulation simpler, the minimum log of BER (minimum LoBER) was used in place of the minimum BER:

$$Min.\, log(BER) = log_{10} B\, ER \qquad (9)$$

the formula for the relationship between the BER and Q-factor is:

$$BER = \frac{1}{2} erfc\left(\frac{Q}{\sqrt{2}}\right) \qquad (10)$$

3. RESULTS AND DISCUSSION

The simulation was performed using the reputable optical system application OptiSystem version 10. The suggested hybrid U-B OCDMA scheme's viability was initially tested based on the architecture shown in Figures 1 and 2. To reduce the nonlinear effect, the power of the CW laser array was reduced to 0 dBm, and one PRBS generator was employed to create the user's information bit at random for transmission over the system.

In the unipolar section, the data bits generated from PRBS generator was modulated with Mach-Zehnder modulator. The modulated signal further amplified with EDFA before combined with bipolar signals and sent through FSO. Further, in the bipolar section, these data bits are sent to the PSK generator with a 0-degree phase offset and delivered as modulation signals after undergoing electrical bias and gain for signal normalization. The optical modulation signals were combined with the information streams using a phase modulator. In addition, 0.5 was chosen as the coupling coefficient for all 2×2 couplers in the simulation. Using a polarization splitter, the signals were split into two orthogonal polarization states (0° and 90°). In this simulation, two optical signals were combined using an optical adder. Two polarization states were combined using a polarization combiner.

A short-to medium-range FSO channel served as the transmission medium in this simulation. In the unipolar section, after passing through FSO, the unipolar signals further filtered out with series of uniform FBG according to the assigned codeword. The optical signals were detected using a photodiode. With a linear phase response cut-off frequency of 0.75*bit rate, a low pass bessel filter was employed. The optical signal was transferred from each port in the bipolar section using an ideal circulator, which stopped it from spreading in an unfavorable way. According to the signature code, the wavelength was reflected and transmitted using a uniform FBG. To finish the bipolar section with balanced photo-detection, two electrical signals were subtracted using an electrical subtractor.

The electrical signals were regenerated using a 3R regenerator. The optical spectra were measured using an optical spectrum analyzer, and the system's output signals were observed using an oscilloscope visualizer. Two of the system performance metrics that were tracked by a BER analyzer in this work were BER and Q-factor. The simulation settings applied to these tests adopted from [22], except for Mach-Zehnder modulator with extinction ratio of 30 dB and erbium-doped fiber amplifier (EDFA) with length of 27m.

The W-H with length 8 was utilized as the signature code. According to Table 1, the codeword $X=[\lambda_2, \lambda_4]$ is assigned to user#1 with a unipolar encoder. Additionally, user#2 with a bipolar encoder is given the codeword $[\lambda_{1H}, \lambda_{3H}]$ for user data bit "0" and $[\lambda_{1V}, \lambda_{3V}]$ for user data bit "1," while user#3 with a bipolar scheme is given the codeword $[\lambda_{1H}, \lambda_{2H}]$ for user data bit "0" and $[\lambda_{1V}, \lambda_{2V}]$ for user data bit "1". By transmitting a series of user data bits with alternating "0" and "1" bits, additional verification was carried out. Figures 3(a), 3(b), and 3(c) show the information generated with PRBS, which produces binary bit sequence between bit "0" and "1" with the matching received signals, for the unipolar and bipolar section of the proposed hybrid U-B OCDMA system's verification.
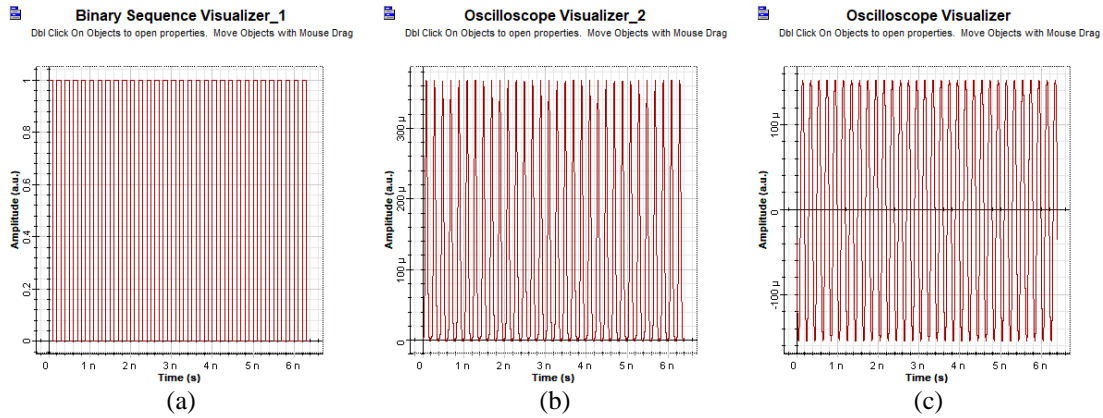
Figure 3. The proposed hybrid U-B OCDMA system's input and output signals for unipolar and bipolar section (a) data from PRBS, (b) received unipolar signals, and (c) received bipolar signals

The MAI reduction feature was assessed using the incompatible condition. The incompatible decoder was demonstrated using the encoder for the unipolar section, which used user#1 signature code from W-H, i.e., (1010), and user#4 signature code from W-H, i.e., (1100). The output following detection in the event of a incompatible decoder where bit "0" was transmitted is shown in Figure 4(a). A small noise-floor signal was measured as a result of the FBG decoder's imperfect filter.

The incompatible decoder was demonstrated for the bipolar section by using user#2 signature code from W-H for the encoder (1100) and user#3 signature code from W-H for the decoder (1001). The output following balanced detection in the case of a incompatible decoder where bit "0" was transmitted is shown in Figure 4(b). A small noise-floor signal was measured as a result of the FBG decoder's imperfect filter. The simulation results demonstrated the viability of the suggested hybrid U-B OCDMA scheme and attested to the system's ability to eliminate MAI.
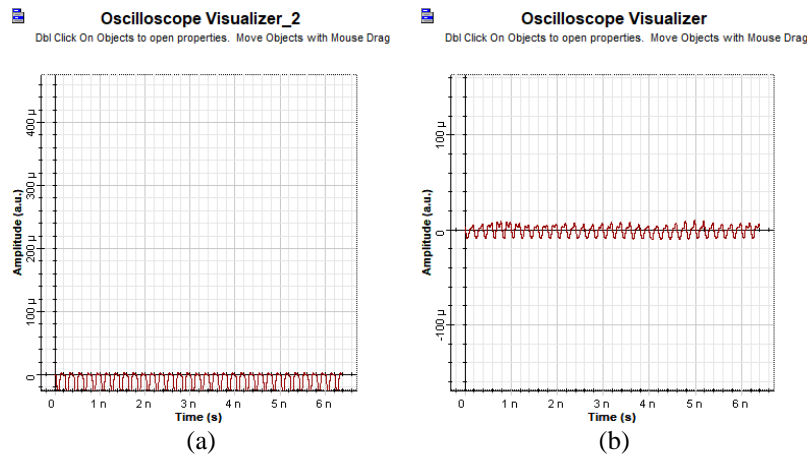
Figure 4. The proposed hybrid U-B OCDMA system output electrical signals when bit "0" was sent, in the (a) unipolar section and (b) bipolar section, for incompatible decoders

To verify the proposed Hybrid OCDMA in various channel conditions, a second simulation was conducted. With three concurrent users, the simulation was done using the architecture shown in Figures 1 and 2. A number of noises were included in the simulation to properly depict the FSO system's surroundings. The noise includes shot noise, thermal noise, and noise from amplified spontaneous emission (ASE), and the overall noise effect can be details in [22]:

$$\sigma_{total}^2 = \sigma_{th}^2 + \sigma_{shot-S}^2 + \sigma_{shot-ASE}^2 + \sigma_{S-ASE}^2 + \sigma_{ASE-ASE}^2 \tag{11}$$

where σ_{total} is total noise, σ_{th} is thermal noise, σ_{shot-S} is shot-signal noise, $\sigma_{shot-ASE}$ is shot-ASE noise, σ_{S-ASE} is signal-ASE noise, and $\sigma_{ASE-ASE}$ is ASE-ASE beat noise.

The AWGN channel and the turbulence channel are the two channel conditions used in this second simulation. A white light source with a power of -130 dBm was included to simulate AWGN channel before the optical signals were carried over the FSO. Additionally, the gamma-gamma distribution was used to describe the turbulence fading channel in this simulation.

The probability of intensity I in the gamma-gamma fading model can be determined by:

$$P(I) = \frac{2(\alpha\beta)^{(\alpha+\beta)/2}}{\Gamma(\alpha)\Gamma(\beta)} I^{(\alpha+\beta)/2-1} K_{\alpha-\beta}\left(2\sqrt{\alpha\beta I}\right) \tag{12}$$

where $\Gamma(\dots)$ is the gamma function and $K_{\alpha-\beta}(\dots)$ is the modified bessel function of the second kind $\frac{1}{\alpha}$ and $\frac{1}{\beta}$ are the variances of the small- and large-scale eddies and can be evaluated with:

$$\alpha = exp\left[\frac{0.49\sigma_R^2}{\left(1+1.11\sigma_R^{12/5}\right)^{5/6}}\right] - 1 \tag{13}$$

$$\beta = exp\left[\frac{0.51\sigma_R^2}{\left(1+0.69\sigma_R^{12/5}\right)^{5/6}}\right] - 1 \tag{14}$$

where σ_R^2 denotes the Rytov variance and is calculated from:

$$\sigma_R^2 = 1.23C_n^2 k^{7/6} z^{11/6} \tag{15}$$

where $C_n^2 C_n^2$ is the parameter index refraction structure with value varies from 10^{-13} m$^{-2/3}$ for strong turbulence to 10^{-17} m$^{-2/3}$ for weak turbulence, k is the optical wavenumber and z is the parameter range.

First, the International Telecommunication Union Radio Communication Sector (ITU-R) P.1817 standard of propagation data required for the construction of terrestrial free-space optical links was used to execute the second simulation in the AWGN channel for certain weather circumstances [25]. In this simulation, three SAC-OCDMA codes-OVSF code, W-H code, and walsh-ZCC code-were used. These codes demonstrate compatibility with the proposed hybrid U-B OCDMA structure by satisfying the correlation properties of (3) and (4). Table 2 displays the signature code that was employed in this simulation where right side used for unipolar section while left side for bipolar section.

Figure 5 shows the performance of the suggested hybrid U-B OCDMA system for AWGN channel in storm weather when using three different codes for the unipolar section. Figure 5(a) presents that for unipolar section in storm conditions, walsh-ZCC code shows best performance in minimum LoBER while other codes got comparable performance. Figure 5(b) presents the max. Q-F for unipolar section in storm conditions, walsh-ZCC code also shows superior performance while other codes achieved quite similar performance. The results of the simulation show that the walsh-ZCC code performed the best, while the OVSF code and the W-H code performed similarly. The storm weather had a greater impact on all codes. Table 3 presents the simulation findings of the AWGN channel's performance deterioration due to weather conditions both for unipolar and bipolar section.

In storm weather conditions for the AWGN channel, Figures 6 shows the performance of hybrid U-B OCDMA system for the bipolar section with three distinct codes. Figure 6(a) depicts the minimum LoBER for bipolar section in storm conditions, W-H code achieved best performance while walsh-ZCC code got highest deterioration performance. Figure 6(b) depicts the maximum Q-F for bipolar section in storm conditions, W-H code also showed greatest performance while walsh-ZCC code suffered highest performance deterioration along with the increasing of FSO range. The results of simulation show that the W-H code performed best. The storm weather had a greater impact on all codes. Walsh-ZCC code experienced the highest performance deterioration due to the rising FSO range.

Table 2. Signature code for hybrid U-B OCDMA system

Code name	Signature code							
OVSF	0	0	1	1	0	0	1	1
	0	1	0	1	0	1	0	1
Walsh-hadamard	1	0	1	0	1	0	1	0
	1	1	0	0	1	1	0	0
Walsh-ZCC	1	0	1	0	0	0	0	1
	1	1	0	0	0	0	1	0

(a)   (b)
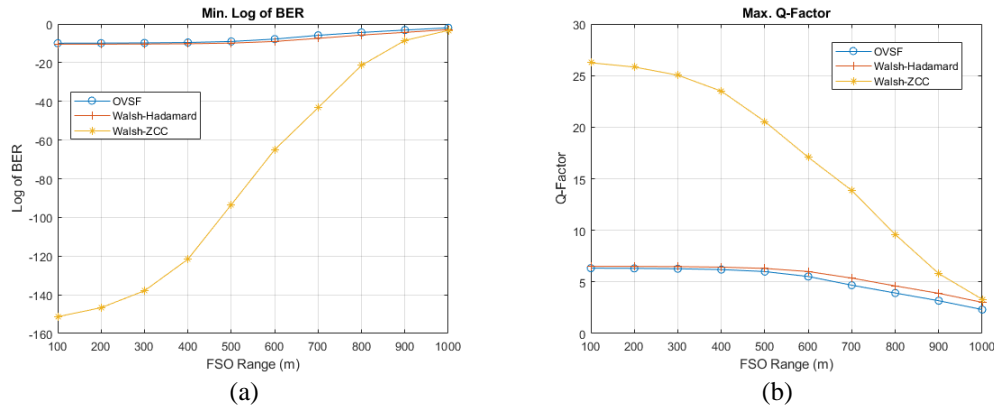
Figure 5. Performance of hybrid U-B OCDMA system for the AWGN channel in storm conditions for the unipolar section (a) minimum LoBER and (b) maximum Q-F

Table 3. Performance deterioration vs FSO range for unipolar and bipolar scheme in AWGN channel with storm weather

Code polarization	Code	Minimum LoBER (a.u.)	Maximum Q-F (a.u.)
Unipolar	OVSF	-7.95542	4.01421
	Walsh-hadamard	-7.53818	3.48766
	Walsh-ZCC	-147.98676	22.92241
Bipolar	OVSF	-11.68538	4.56223
	Walsh-hadamard	-11.73894	4.46522
	Walsh-ZCC	-13.45761	5.96944

(a)   (b)
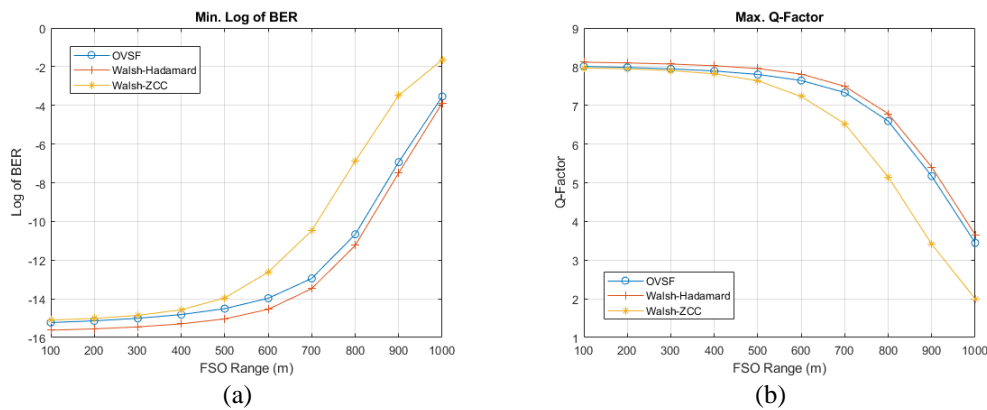
Figure 6. Performance of hybrid U-B OCDMA system for the AWGN channel in storm conditions for the bipolar section (a) minimum LoBER and (b) maximum Q-F

The following simulation added turbulence fading to the channel under strong turbulence conditions based on (12), in addition to AWGN effects. Simulations for extreme weather were also conducted. Figures 7 shows the minimum LoBER and maximum Q-F for the AWGN and turbulence channel in the unipolar section for each code during storm weather. Figure 7(a) shows the minimum LoBER for unipolar section in storm conditions, walsh-ZCC code achieved superior performance but suffered highest deterioration performance. Figure 7(b) shows the maximum Q-F for unipolar section in storm conditions, walsh-ZCC code also got greatest performance although got highest performance deterioration along with the increasing of FSO range. Based on the simulation results, the walsh-ZCC code outperformed the other codes while maintaining a same level of performance. Walsh-ZCC code was badly harmed by optical signal attenuation in the storm weather because it continued to perform worse than other codes despite still outperforming them in these two weather scenarios.
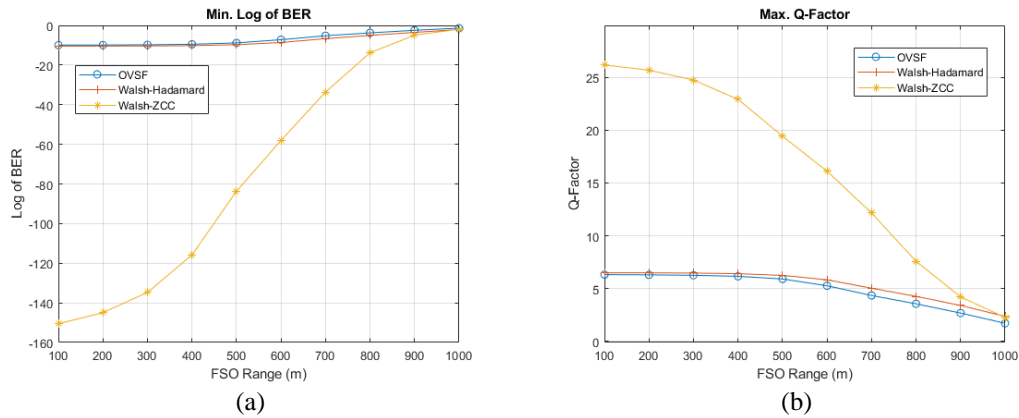
Figure 7. Performance of hybrid U-B OCDMA system for the AWGN and turbulence channel during storm for the unipolar section (a) minimum LoBER and (b) maximum Q-F

For AWGN and turbulence channels, respectively, Figures 8 illustrate the minimum Log of BER and maximum Q-Factor for each code during storm weather. Figure 8(a) demonstrates the minimum LoBER for bipolar section in storm conditions, W-H code reached highest performance while walsh-ZCC code suffered highest deterioration performance. Figure 8(b) demonstrates the maximum Q-F for bipolar section in storm conditions, W-H code also had superior performance and walsh-ZCC code suffered highest performance deterioration along with the increasing of FSO range. The W-H code, followed by the OVSF code and the walsh-ZCC code, had the best performance, according to the findings of the simulation. The walsh-ZCC code still showed the worst performance decrease in this weather conditions when compared to other codes. Table 4 shows the simulation findings for performance loss due to weather condition in the AWGN and turbulence channel for unipolar and bipolar section.
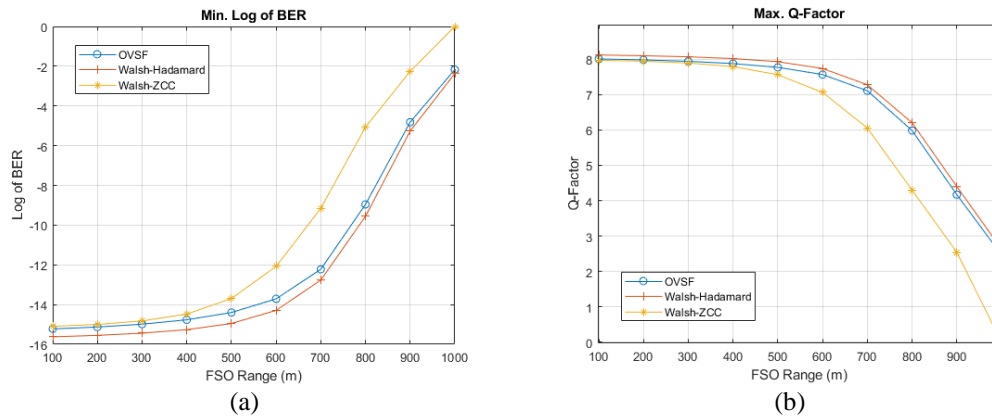
Figure 8. Performance of hybrid U-B OCDMA system for the AWGN channel in storm conditions for the bipolar section (a) minimum LoBER and (b) maximum Q-F

The suggested hybrid U-B OCDMA system was put to the test in the final simulations under turbulence scenarios. Figure 9 depicts various SAC codes implemented in the suggested hybrid U-B OCDMA system function under strong turbulence circumstances based on (12) for unipolar section. Figure 9(a) presents the minimum LoBER for unipolar section in strong turbulence conditions, walsh-ZCC code showed superior performance while other codes had comparable performance. Figure 9(b) presents the maximum Q-F for unipolar section in strong turbulence conditions, walsh-ZCC code also got highest performance and other code had similar performance. From the simulation results, W-H code had the comparable performance with OVSF, while walsh-ZCC code presents the best performance. Walsh-ZCC code has an 800 m maximum range in strong turbulence, while OVSF code and W-H code systems can achieve 900 m.

Table 4. Performance deterioration vs FSO range for unipolar and bipolar scheme in AWGN and turbulence
channel with storm weather

Code polarization	Code	Minimum LoBER (a.u.)	Maximum Q-F (a.u.)
Unipolar	OVSF	-8.57289	4.60553
	Walsh-hadamard	-8.38292	4.12771
	Walsh-ZCC	-148.61361	23.8992
Bipolar	OVSF	-13.05608	5.53623
	Walsh-hadamard	-13.252	5.4851
	Walsh-ZCC	-15.0951	7.96694

(a)   (b)
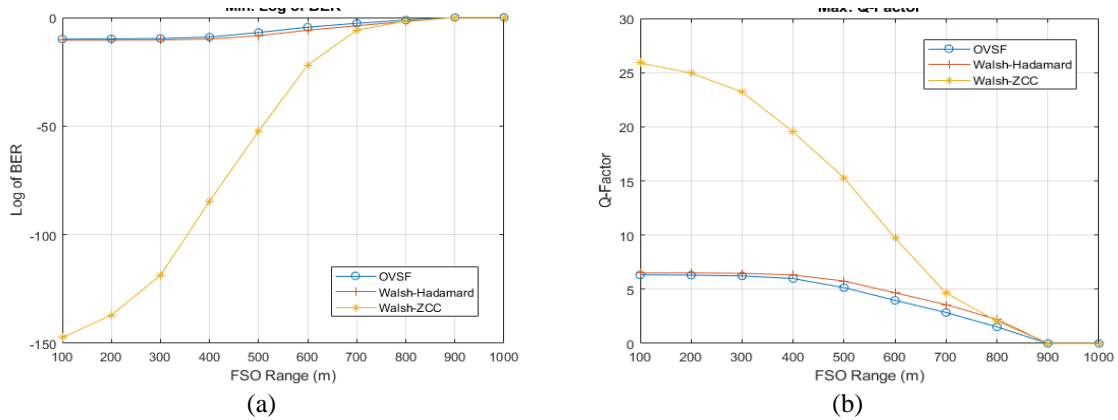
Figure 9. Performance of hybrid U-B OCDMA system in strong turbulence conditions for the unipolar
section (a) minimum LoBER and (b) maximum Q-F

Based on (12) for the bipolar section, Figure 10 illustrates how various SAC codes implemented in
the suggested hybrid U-B OCDMA system perform under turbulence conditions. Figure 10(a) depicts the
minimum LoBER for bipolar section in strong turbulence conditions, W-H code showed best performance
while other codes had comparable performance. Figure 10(b) presents the maximum Q-F for bipolar section in
strong turbulence conditions, W-H code also achieved superior performance and other code had quite similar
performance. The simulation results showed that W-H code had the best performances. In the suggested hybrid
U-B OCDMA system, walsh-ZCC code proved its suitability for short to medium distance FSO by
demonstrating the greatest performance deterioration vs FSO range under turbulence conditions. Walsh-ZCC
code has an 800 m maximum range in conditions of strong turbulence, while OVSF code and W-H code
systems can achieve 900m. Table 5 showed the simulation findings of performance decrease for various
turbulence situations in the unipolar and bipolar section.

(a)   (b)
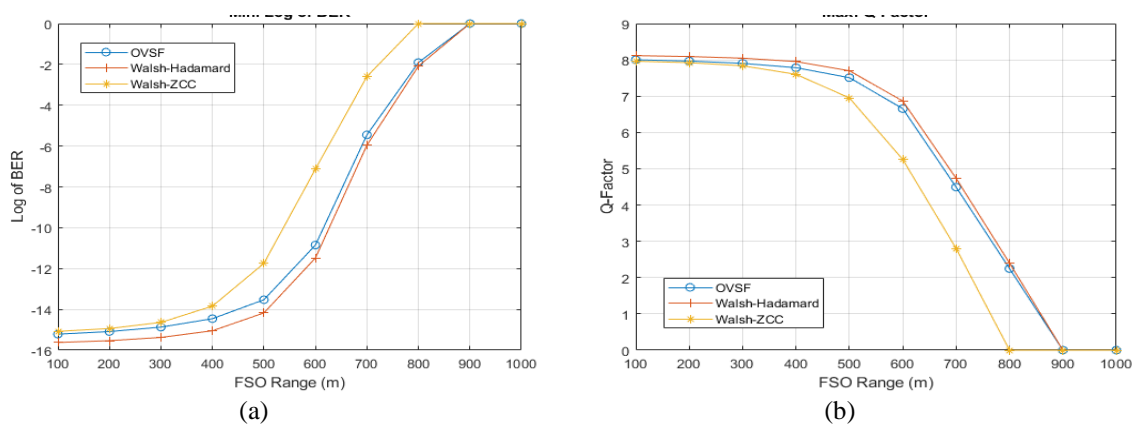
Figure 10. Performance of hybrid U-B OCDMA system in strong turbulence conditions for the bipolar
section (a) minimum LoBER and (b) maximum Q-F

Table 5. Degradation in performance vs FSO range for unipolar and bipolar section in strong turbulence conditions

Code polarization	Code	Minimum LoBER (a.u.)	Maximum Q-F (a.u.)
Unipolar	OVSF	-9.94339	6.32929
	Walsh-hadamard	-10.4615	6.51054
	Walsh-ZCC	-147.371	25.8902
Bipolar	OVSF	-15.2151	8.0025
	Walsh-hadamard	-15.6222	8.11594
	Walsh-ZCC	-15.0774	7.96191

4. CONCLUSION

This study successfully developed and proved the viability of hybrid U-B OCDMA with combined unipolar-bipolar system in FSO communication with short- to medium-range. The observation from the simulation shows that the suggested hybrid U-B OCDMA can correctly decode the original signal from both the unipolar and bipolar section. The original SAC-OCDMA approaches, which in theory mitigate the MAI effect, served as the foundation for the proposed system's design. The simultaneous transmission of medium-low and high-rate data can be accommodated by the hybrid U-B OCDMA system that is being suggested. Additionally, the codeword assigned introduced the quasi-polarized code, which could be used to both the unipolar and bipolar section. Three alternative OCDMA codes were used to mimic the performance measurements in severe weather conditions, first for the AWGN channel and then for the AWGN and turbulence channel. Additional testing of the proposed hybrid U-B OCDMA system was done under strong turbulence conditions. According to the simulation results, walsh-ZCC outperforms all other codes for the unipolar section whereas W-H code performs best for the bipolar section. In every weather and turbulence scenario, the simulations also showed that the walsh-ZCC code had the greatest performance decrease. This result indicated that Walsh-ZCC code can be employed most effectively for unipolar section in the proposed hybrid U-B OCDMA system's short-to-medium-range FSO application. These findings can be considered in code selection.

Future studies can look at the recommended hybrid U-B OCDMA technique for long-range OWC in connection to different atmospheric situations to support a greater multi-user scheme. It is possible to further increase performance using a variety of optimization strategies. Additionally, a new code that works effectively with hybrid schemes can be suggested.

ACKNOWLEDGEMENTS

REFERENCES

[1] M. Banafaa *et al.*, "6G Mobile Communication Technology: Requirements, Targets, Applications, Challenges, Advantages, and Opportunities," *Alexandria Engineering Journal*, vol. 64, pp. 245–274, 2023, doi: 10.1016/j.aej.2022.08.017.

[2] M. Z. Chowdhury, M. Shahjalal, S. Ahmed, and Y. M. Jang, "6G Wireless Communication Systems: Applications, Requirements, Technologies, Challenges, and Research Directions," *IEEE Open Journal of the Communications Society*, vol. 1, pp. 957–975, 2020, doi: 10.1109/OJCOMS.2020.3010270.

[3] Z. Wei, Z. Wang, J. Zhang, Q. Li, J. Zhang, and H. Y. Fu, "Evolution of optical wireless communication for B5G/6G," *Progress in Quantum Electronics*, vol. 83, p. 100398, 2022, doi: 10.1016/j.pquantelec.2022.100398.

[4] A. Fayad, T. Cinkler, J. Rak, and M. Jha, "Design of Cost-Efficient Optical Fronthaul for 5G/6G Networks: An Optimization Perspective," *Sensors*, vol. 22, no. 23, p. 9394, 2022, doi: 10.3390/s22239394.

[5] M. Giordani, M. Polese, M. Mezzavilla, S. Rangan, and M. Zorzi, "Toward 6G Networks: Use Cases and Technologies," *IEEE Communications Magazine*, vol. 58, no. 3, pp. 55–61, 2020, doi: 10.1109/MCOM.001.1900411.

[6] P. Yang, Y. Xiao, M. Xiao, and S. Li, "6G Wireless Communications: Vision and Potential Techniques," *IEEE Network*, vol. 33, no. 4, pp. 70–75, 2019, doi: 10.1109/MNET.2019.1800418.

[7] A. Malik and P. Singh, "Free Space Optics: Current Applications and Future Challenges," *International Journal of Optics*, vol. 2015, pp. 1–7, 2015, doi: 10.1155/2015/945483.

[8] L. U. Khan, I. Yaqoob, M. Imran, Z. Han, and C. S. Hong, "6G Wireless Systems: A Vision, Architectural Elements, and Future Directions," *IEEE Access*, vol. 8, pp. 147029–147044, 2020, doi: 10.1109/ACCESS.2020.3015289.

[9] S. R. Gopalan, H. Chandran, B. S. Ranganath, and K. A. Saketh, "Nonlinear effects on WDM optical communication system," *Journal of Optical Communications*, 2022, doi: 10.1515/joc-2022-0005.

[10] M. A. Saleh, A. K. Abass, and M. H. Ali, "Enhancing performance of WDM-RoFSO communication system utilizing dual channel technique for 5G applications," *Optical and Quantum Electronics*, vol. 54, no. 8, p. 497, 2022, doi: 10.1007/s11082-022-03857-8.

[11] J. G. Zhang and A. B. Sharma, "High-Speed Optical Time-Division Multiple-Access (OTDMA) Networks Using Optical Signal Processing," *Photonic Network Communications*, vol. 1, no. 4, pp. 273–285, 1999, doi: 10.1023/A:1010070632272.

[12] H. Z. Dhaam, M. J. A. Dujaili, M. T. Mezeel, and A. A. Qasim, "Performance of high scalability hybrid system of 10G-TDM-OCDMA-PON based on 2D-SWZCC code," *Journal of Optical Communications*, vol. 44, no. s1, pp. s1121–s1129, 2021, doi: 10.1515/joc-2021-0075.

[13]   M. N. H. Prince, M. Faisal, and S. P. Majumder, "Performance analysis of an optical TDM transmission link considering fiber dispersion and demultiplexer crosstalk," *Optik*, vol. 251, p. 168435, 2022, doi: 10.1016/j.ijleo.2021.168435.

[14]   C. Rashidi and S. Aljunid, "Phase Induced Intensity Noise Evasion in SAC-OCDMA Systems Using Flexible Cross Correlation (FCC) Code Algorithm," *Australian Journal of Basic and Applied Sciences*, vol. 7, no. 8, pp. 437–446, 2013.

[15]   L. Bouhezila, A. Bouarfa, A. Garadi, and A. Bensaad, "Cardinality increasing of SAC-OCDMA system using novel decoder design," *Journal of Optical Communications*, 2023, doi: 10.1515/joc-2022-0150.

[16]   M. Singh, J. Kříž, M. M. Kamruzzaman, V. Dhasarathan, A. Sharma, and S. A. Abd El-Mottaleb, "Design of a High-Speed OFDM-SAC-OCDMA-Based FSO System Using EDW Codes for Supporting 5G Data Services and Smart City Applications," *Frontiers in Physics*, vol. 10, 2022, doi: 10.3389/fphy.2022.934848.

[17]   H. M. R. Al-Khafaji, S. A. Aljunid, and H. A. Fadhil, "Spectral efficiency analysis of bipolar spectralamplitude coding optical code-division multipleaccess systems using different one-dimensional codes," *IET Optoelectronics*, vol. 6, no. 5, pp. 215–222, 2012, doi: 10.1049/iet-opt.2011.0051.

[18]   A. Farhat, M. Menif, C. Lepers, H. Rezig, and P. Gallion, "Comparison of unipolar codes for DS-OCDMA system," in *International Conference on Transparent Optical Networks Mediterranean Winter*, IEEE, pp. 1–4, 2008, doi: 10.1109/ICTONMW.2008.4773064.

[19]   H. M. R. Al-Khafaji, S. A. Aljunid, and H. A. Fadhil, "Spectral efficiency comparison of SAC-OCDMA systems using unipolar and bipolar encoding techniques," in *Conference Proceedings-2011 IEEE 2nd International Conference on Photonics*, IEEE, pp. 1–5, 2011, doi: 10.1109/ICP.2011.6106822.

[20]   H. C. Cheng, E. Wijanto, T. C. Lien, P. H. Lai, and S. P. Tseng, "Multiple access techniques for bipolar optical code division in wireless optical communications," *IEEE Access*, vol. 8, pp. 83511–83523, 2020, doi: 10.1109/ACCESS.2020.2991071.

[21]   S. P. Tseng, E. Wijanto, P. H. Lai, and H. C. Cheng, "Bipolar optical code division multiple access techniques using a dual electro-optical modulator implemented in free-space optics communications," *Sensors (Switzerland)*, vol. 20, no. 12, pp. 1–14, 2020, doi: 10.3390/s20123583.

[22]   E. Wijanto and C. M. Huang, "Design of bipolar optical code-division multiple-access techniques using phase modulator for polarization coding in wireless optical communication," *Applied Sciences (Switzerland)*, vol. 11, no. 13, p. 5955, 2021, doi: 10.3390/app11135955.

[23]   A. K. M. N. Islam and S. P. Majumder, "Effect of atmospheric turbulence on the BER performance of an optical CDMA FSO link with SIK receiver," *Optik*, vol. 179, pp. 867–874, 2019, doi: 10.1016/j.ijleo.2018.08.008.

[24]   A. Aissaoui and L. Hacini, "Performance Comparison of Different SAC-OCDMA-FSO Detection Techniques in Presence of Atmospheric Losses," in *International Conference on Image and Signal Processing and their Applications*, IEEE, pp. 1–5, 2019, doi: 10.1109/ISPA48434.2019.8966876.

[25]   ITUR, "P.1817 Propagation data required for the design of terrestrial free-space optical links," *ITU-Recommendation*, vol. 1, 2012.

BIOGRAPHIES OF AUTHORS

Eddy Wijanto 🆔 📇 SC ⬡ received his BS degree from the Department of Electrical Engineering at Krida Wacana Christian University, Indonesia, in 2005, his M.S. degrees from the Department of Electrical Engineering, Pelita Harapan University, Indonesia, in 2009, and his Ph.D. degrees from the Electro-Optical Engineering Department at National Formosa University, Yunlin County, Taiwan, R.O.C, in 2021. He received his Professional Engineer from Atma Jaya Indonesia Catholic University, in 2023. He is currently an Associate Professor at the Department of Electrical Engineering, Krida Wacana Christian University, Indonesia. His major interests are mainly in the areas of wireless and optical communications. He can be contacted at email: eddy.wiyanto@ukrida.ac.id.

Kevin Sutanto 🆔 📇 SC ⬡ received his BS degree from the Department of Electrical Engineering at Krida Wacana Christian University, Indonesia, in 2019, his M.S. degree from the Department of Electronics Engineering, Ming-Chi University of Technology, Taiwan, in 2022. He is currently a Lecturer at the Department of Electrical Engineering, Krida Wacana Christian University, Indonesia. His major interests are mainly in the areas of artificial intelligence and computer vision. He can be contacted at email: kevin.sutanto@ukrida.ac.id.